11th World Congress on Computational Mechanics (WCCM XI)
5th European Conference on Computational Mechanics (ECCM V)
6th European Conference on Computational Fluid Dynamics (ECFD VI)
E. Oñate, J. Oliver and A. Huerta (Eds)

NON-LINEAR ANALYSIS OF STEEL-CONCRETE BEAMS USING GENERALIZED BEAM THEORY

DAVID HENRIQUES*, RODRIGO GONÇALVES* AND DINAR CAMOTIM†

* UNIC, Civil Engineering Department, Faculdade de Ciências e Tecnologia, Universidade Nova de Lisboa, 2829-516 Caparica, Portugal
e-mail: rodrigo.goncalves@fct.unl.pt

† ICIST, Department of Civil Engineering, Architecture and Georesources, Instituto Superior Técnico, University of Lisbon, Av. Rovisco Pais, 1049-001 Lisbon, Portugal
e-mail: dcamotim@civil.ist.utl.pt

Key words: Steel-concrete composite beams, Generalized Beam Theory (GBT), Cross-section deformation, Non-linear behaviour.

Abstract. In recent papers, the authors have presented Generalized Beam Theory (GBT) formulations specifically designed for performing efficient (i) linear analyses of steel-concrete composite bridges [1] and (ii) elastoplastic collapse analyses of thin-walled steel members [2, 3]. This paper presents an extension of these previous formulations that includes non-linear reinforced concrete material behaviour, aiming at analysing, accurately and efficiently, steel-concrete composite beams. In particular, steel beam and rebar plastification is implemented, together with concrete cracking/crushing and shear-lag effects. Several illustrative examples are presented and discussed. For validation and comparison purposes, results obtained with shell/solid finite element models are provided.

1 Introduction

The Generalized Beam Theory (GBT), first proposed by Schardt [4], may be viewed as an extension of Vlasov's prismatic bar theory that takes into account cross-section in-plane and out-of-plane (warping) deformation through the consideration of pre-determined "cross-section deformation modes", whose amplitudes along the beam axis constitute the only problem unknowns. It has been widely demonstrated that GBT constitutes a powerful, elegant and clarifying tool to solve a wide range of structural problems involving prismatic thin-walled members (e.g., [5]).

Recently, in the field of steel-concrete composite bridge linear analyses, very promising results have been obtained with GBT, due to its straightforward capability of including

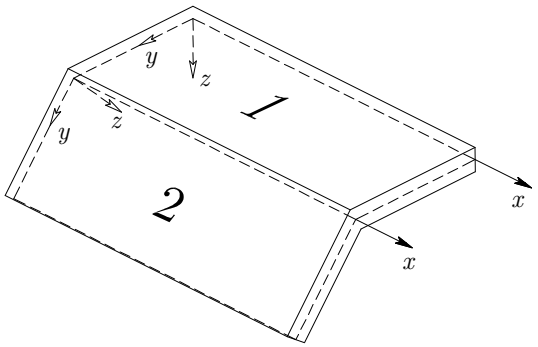

Figure 1: Arbitrary thin-walled member geometry and local coordinate ystems.

shear-lag and shear connection flexibility effects [1]. In addition, elastoplastic GBT formulations (either geometrically linear or non-linear) have also been developed [2, 3]. In this paper, an extension of these previous formulations is presented, which aims at modelling the materially non-linear behaviour of steel-concrete composite beams. In particular, a GBT-based finite element is presented, which incorporates (i) reinforced concrete non-linear behaviour, (ii) shear-lag effects and (iii) steel beam plasticity. A trade-off between accuracy and computational efficiency is achieved by taking advantage of the inherent features of GBT: shear deformation is allowed for through the inclusion of appropriate deformation modes, while the stress and strain fields are constrained in order to limit the number of d.o.f. involved and also to make it possible to employ a simple concrete material model.

2 Fundamental aspects of the GBT-based beam finite element

The beam finite element corresponds to the geometrically linear version of the element presented in [3]. Making reference to Fig. 1, where x, y and z are wall mid-surface local axes, the GBT wall displacement vector $\boldsymbol{U}(x,y,z)$ is given by

$$\boldsymbol{U}(x,y,z) = \left(\bar{\boldsymbol{\Xi}}_U(y) + z\boldsymbol{\Xi}_U(y)\right) \begin{bmatrix} \boldsymbol{\phi}(x) \\ \boldsymbol{\phi}_{,x}(x), \end{bmatrix}, \tag{1}$$

$$\bar{\boldsymbol{\Xi}}_U(y) = \begin{bmatrix} \mathbf{0} & \bar{\boldsymbol{u}}^t \\ \bar{\boldsymbol{v}}^t & \mathbf{0} \\ \bar{\boldsymbol{w}}^t & \mathbf{0} \end{bmatrix}, \quad \boldsymbol{\Xi}_U(y) = - \begin{bmatrix} \mathbf{0} & \bar{\boldsymbol{w}}^t \\ \bar{\boldsymbol{w}}^t_{,y} & \mathbf{0} \\ \mathbf{0} & \mathbf{0} \end{bmatrix}, \tag{2}$$

where $\boldsymbol{\phi}(x)$ is a column vector containing the deformation mode amplitude functions along x (the unknowns), the comma indicates a differentiation and $\bar{\boldsymbol{u}}(y)$, $\bar{\boldsymbol{v}}(y)$, $\bar{\boldsymbol{w}}(y)$ are column vectors containing the deformation mode displacement components of the cross-section mid-line along x, y and z, respectively.

The non-null small strain components are given by $\boldsymbol{\varepsilon}^t = [\varepsilon_{xx}\ \varepsilon_{yy}\ \gamma_{xy}]$, which may be

subdivided into membrane/bending terms, obtained from the matrix equations

$$\boldsymbol{\varepsilon} = \boldsymbol{\varepsilon}^M + \boldsymbol{\varepsilon}^B = \left(\boldsymbol{\Xi}_{\varepsilon}^M + z\boldsymbol{\Xi}_{\varepsilon}^B\right) \begin{bmatrix} \boldsymbol{\phi} \\ \boldsymbol{\phi}_{,x} \\ \boldsymbol{\phi}_{,xx} \end{bmatrix}, \tag{3}$$

$$\boldsymbol{\Xi}_{\varepsilon}^M = \begin{bmatrix} \mathbf{0} & \mathbf{0} & \bar{\boldsymbol{u}}^t \\ \bar{\boldsymbol{v}}_{,y}^t & \mathbf{0} & \mathbf{0} \\ \mathbf{0} & (\bar{\boldsymbol{u}}_{,y} + \bar{\boldsymbol{v}})^t & \mathbf{0} \end{bmatrix}, \; \boldsymbol{\Xi}_{\varepsilon}^B = - \begin{bmatrix} \mathbf{0} & \mathbf{0} & \bar{\boldsymbol{w}}^t \\ \bar{\boldsymbol{w}}_{,yy}^t & \mathbf{0} & \mathbf{0} \\ \mathbf{0} & 2\bar{\boldsymbol{w}}_{,y}^t & \mathbf{0} \end{bmatrix}. \tag{4}$$

The non-null stresses are given by vector $\boldsymbol{\sigma}^t = [\sigma_{xx} \; \sigma_{yy} \; \sigma_{xy}]$ and are calculated from the particular constitutive relations adopted. However, with the purpose of avoiding the use of complex constitutive models, the stress and strain fields are constrained through $\sigma_{yy} = \sigma_{xy}^B = 0$ and $\varepsilon_{yy} = \gamma_{xy}^B = 0$. These constraints also have the advantage of limiting the number of deformation modes (i.e., d.o.f.) necessary to achieve accurate results. As a consequence, besides the usual axial extension and Euler-Bernoulli bending deformation modes, only a reduced set of warping modes needs to be included in the analyses, which the purpose of capturing shear deformation in the steel web and concrete slab.

For elastic strains, a St. Venant-Kirchhoff material law is assumed, with $\sigma_{xx} = E\varepsilon_{xx}$ and $\sigma_{xy} = G\gamma_{xy}$, where E and G are Young's and shear moduli. For the steel beam, the Mises yield function with associated flow rule is employed. The stresses at the end of each iteration are updated using the backward-Euler return algorithm for plane stress with the $\sigma_{yy} = 0$ constraint and the related consistent constitutive matrix is employed (see, for example, [6]). The longitudinal steel rebars are smeared, along y, at any given layer z of the slab and a perfect bond is assumed. In this case, an uniaxial elastic-perfectly plastic material law is employed. For concrete, an uniaxial law is adopted for σ_{xx}, without tensile strength and a non-linear compressive branch. This implies that cracks always develop along the y direction. The shear stresses are given by $\sigma_{xy} = G\gamma_{xy}$, unless cracking occurs and, in this case, $\sigma_{xy} = \beta G\gamma_{xy}$, where β is the shear retention factor.

The beam finite element is obtained by interpolating the amplitude functions $\boldsymbol{\phi} = \boldsymbol{\Psi}\boldsymbol{d}$, where matrix $\boldsymbol{\Psi}$ contains the interpolation functions and vector $\boldsymbol{d}$ contains the unknowns (nodal values of the amplitude functions). Both Hermite (cubic) and Lagrange quadratic functions are employed, with the latter used only for the warping deformation modes. The out-of-balance force vector $\boldsymbol{g}$, the tangent stiffness matrix $\boldsymbol{K}_t$ and the incremental load vector $\Delta\boldsymbol{f}$ are given by

$$\boldsymbol{g} = \int_V \begin{bmatrix} \boldsymbol{\Psi} \\ \boldsymbol{\Psi}_{,x} \\ \boldsymbol{\Psi}_{,xx} \end{bmatrix}^t \boldsymbol{\Xi}_{\varepsilon}^t \, \boldsymbol{\sigma} \, dV - \int_\Omega \begin{bmatrix} \boldsymbol{\Psi} \\ \boldsymbol{\Psi}_{,x} \end{bmatrix}^t \bar{\boldsymbol{\Xi}}_U^t \, \bar{\boldsymbol{q}} \, d\Omega, \tag{5}$$

$$\boldsymbol{K}_t = \int_V \begin{bmatrix} \boldsymbol{\Psi} \\ \boldsymbol{\Psi}_{,x} \\ \boldsymbol{\Psi}_{,xx} \end{bmatrix}^t \boldsymbol{\Xi}_{\varepsilon}^t \, \boldsymbol{C}_t \, \boldsymbol{\Xi}_{\varepsilon} \begin{bmatrix} \boldsymbol{\Psi} \\ \boldsymbol{\Psi}_{,x} \\ \boldsymbol{\Psi}_{,xx} \end{bmatrix} dV, \tag{6}$$

$$\Delta\boldsymbol{f} = \int_\Omega \begin{bmatrix} \boldsymbol{\Psi} \\ \boldsymbol{\Psi}_{,x} \end{bmatrix}^t \bar{\boldsymbol{\Xi}}_U^t \, \Delta\bar{\boldsymbol{q}} \, d\Omega, \tag{7}$$

where $\bar{\boldsymbol{q}}$ are forces acting along the walls mid-surface Ω and $\boldsymbol{C}_t$ is the (consistent) tangent constitutive matrix. Numerical integration is performed using 3 Gauss points along x and y, in each wall, and 2 Gauss points along z (except where mentioned).

3 Illustrative examples

3.1 Example 1

The first example provides evidence of the accuracy of the proposed element in the determination of elastic longitudinal normal stresses (σ_{xx}) due to shear-lag. Two simply supported twin-beams are analysed, with length L equal to 6 and 8 m — the cross-section geometry and the material parameters are given in Fig. 2(a). The beams are subjected to sagging bending, induced by 1 kN/m uniformly distributed loads acting in the plane of the steel webs. Due to the problem double symmetry, only a quarter of the twin-beams is modelled (half of the length/cross-section).

The GBT analyses are carried out with 7 deformation modes, which are determined using the cross-section "frame" shown in Fig. 2(b) and correspond to (see Fig. 2(c)): (1) axial extension, (2) bending, (3) warping associated with bending, (4-5) linear and (6-7) quadratic warping in each concrete flange. The longitudinal discretization involved 8 equal length finite elements, which amounts to 112 d.o.f..

For comparison purposes, a refined shell finite element model is also analysed, using ADINA [7] — the mesh is shown in Fig. 2(d).

The GBT analysis yielded vertical displacements at mid-span equal to $1.27/3.39 \times 10^{-5}$ ($L = 6/8$ m), which are within 1.6% of the shell model results ($1.29/3.34 \times 10^{-5}$). Furthermore, Figs. 3(a-b) show the GBT-based deformed configurations and σ_{xx} distributions in the concrete flanges — note that, naturally, the shear-lag effect is more pronounced for the shorter span ($L = 6$ m). The graphs (c) in the figure detail the σ_{xx} distributions at mid-span, making it possible to conclude that there is an excellent match between the GBT and shell model results.

Finally, the graphs (d) in Fig. 3 plot the mode amplitude functions along x. It is observed that, for the shorter span, there is a significant participation of the bending warping mode, which reveals shear deformation of the steel web near the support. Concerning the shear-lag modes, it is concluded that, for both spans, the linear modes are the most relevant. One final word to mention that the participations of the axial mode are non-null due to the fact that the shear-lag modes introduce axial force.

3.2 Example 2

The second example includes concrete cracking, although the materials are otherwise assumed elastic. A 8.0 m length composite beam is considered, with one end simply supported and the other built-in — the cross-section geometric and material parameters are shown in Fig. 4(a). As in the previous example, a 1 kN/m uniformly distributed load is applied in the plane of the steel web.

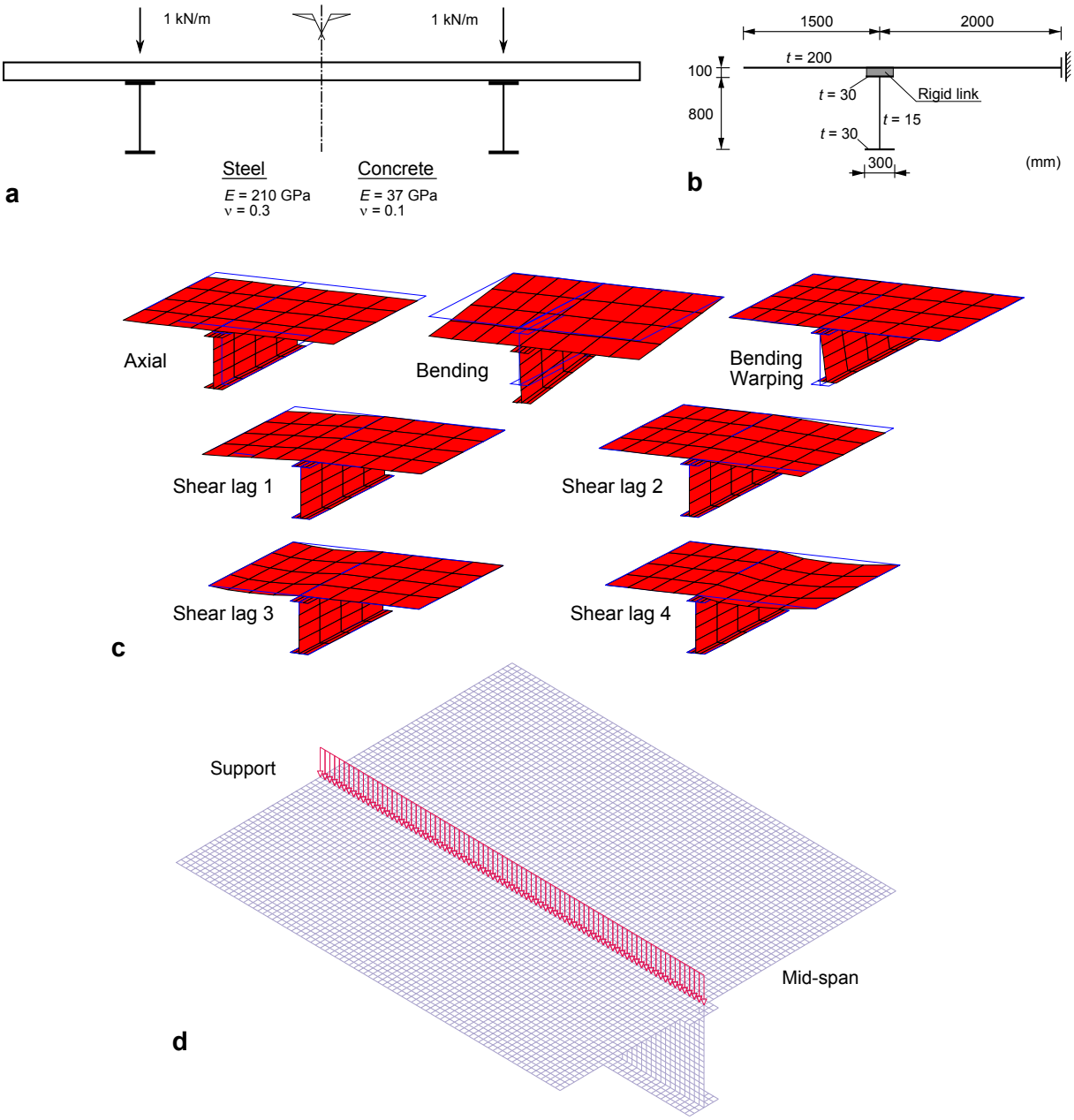

Figure 2: Example 1: (a) cross-section geometry, loading and material parameters, (b) equivalent "frame" for the GBT cross-section analysis, (c) deformation modes and (d) shell finite element model.

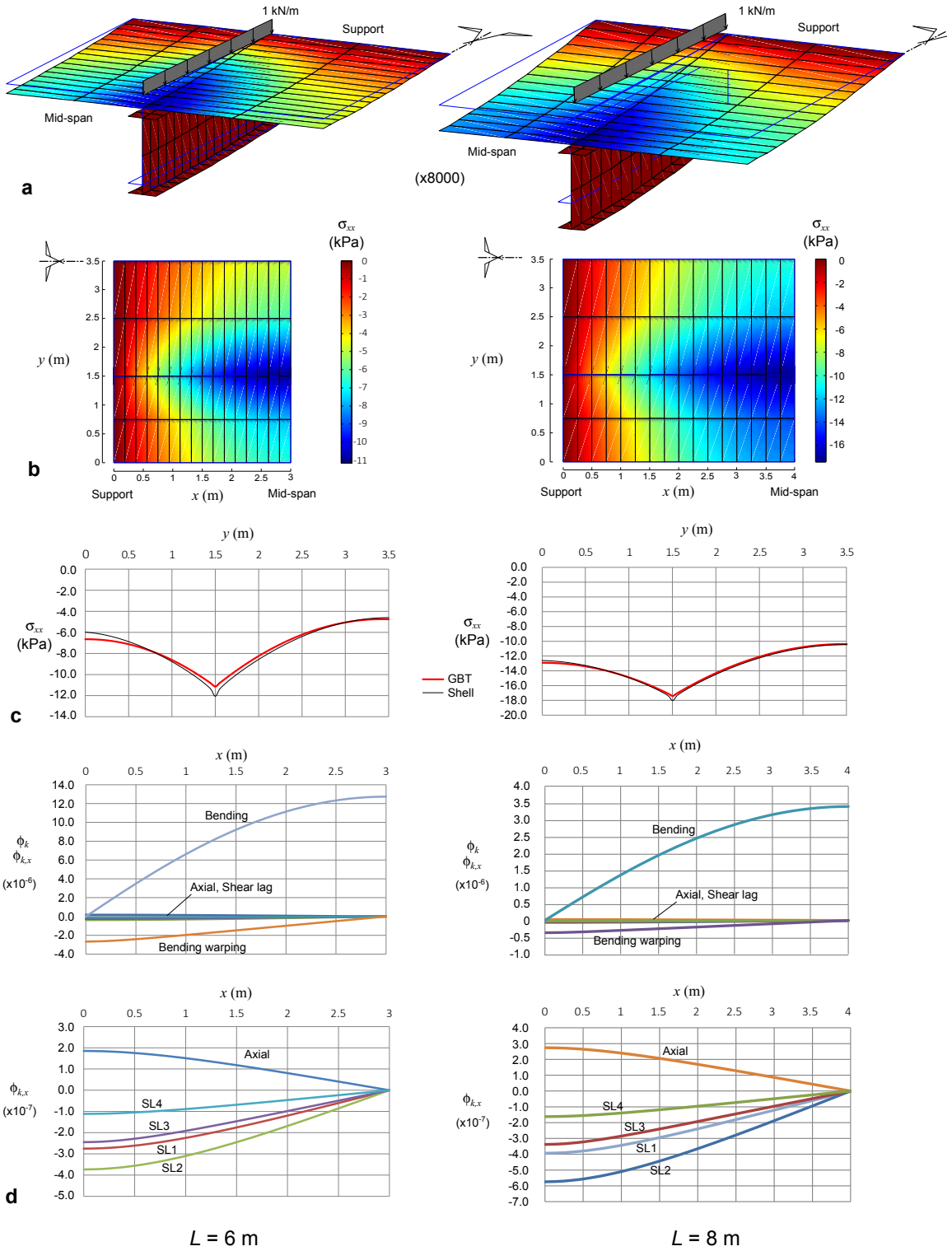

Figure 3: Example 1: (a) deformed configurations, (b) stresses in the concrete slab, (c) stresses at midspan and (d) deformation mode amplitude functions along x.

For the GBT analyses, due to the cross-section symmetry, only two shear-lag deformation modes are considered, with linear and quadratic warping functions in the concrete flanges (see Fig. 4(b)). Two discretisation levels are adopted, using 8/64 equal length elements. In each case, two values for β are considered: 1/3 and 1.0.

For comparison purposes, the standard finite element model shown in Fig. 4(c) is also analysed, which involves (i) shell elements for the steel beam, (ii) truss elements for the individual steel rebars and (iii) 3D-solid elements for the concrete slab with the ADINA concrete material model and $\beta = 1/3$.

Table 1 provides the obtained vertical displacements at mid-span. Clearly, the GBT results are virtually unaffected by the β value (differences below 0.4%) and 8 finite elements already lead to satisfactory results — with 64 elements the displacement increases by only 1.5%. The shell/truss/solid element model is slightly stiffer, yielding a displacement which is about 6% below the GBT solutions.

Table 1: Example 2: Vertical displacement at mid-span

GBT, 8 FE		GBT, 64 FE		Shell/Solid
$\beta = 1.0$	$\beta = 1/3$	$\beta = 1.0$	$\beta = 1/3$	$\beta = 1/3$
2.296×10^{-5}	2.304×10^{-5}	$2.331\ \times10^{-5}$	2.332×10^{-5}	2.183×10^{-5}

Fig. 5 provides detailed GBT results, namely the deformed configurations and the stress distributions in the concrete (discretization with 8 elements and $\beta = 1$), as well as the mode amplitude functions for the two discretizations and β values considered. The stress distributions clearly show cracking near the built-in support and shear-lag effects. Concerning the mode amplitude function graphs, it is observed that the beam behaviour is mainly governed by bending, but web shear deformation also plays a significant role. Of the two shear-lag modes, the quadratic one (SL2) has the most relevant participation. This mode exhibits a rather complex variation near the built-in end, which can only be adequately captured using 64 elements. Finally, note that a reduction of the β value leads to an increase of the participation of the shear-lag modes in the hogging region.

3.3 Example 3

A two-span beam tested by Ansourian [8] is now analysed. This example was also examined in [9], using a beam finite element. The loading and geometric/material parameters are indicated in Fig. 6(a). In this case, shear-lag and web shear deformation are not relevant, but steel plasticity and concrete non-linear behaviour must be taken into consideration, in order to obtain the non-linear load-displacement curve up to collapse.

The GBT analyses only require including two deformation modes, bending and axial extension. As in [9], the uniaxial law for concrete in compression is given by (all values

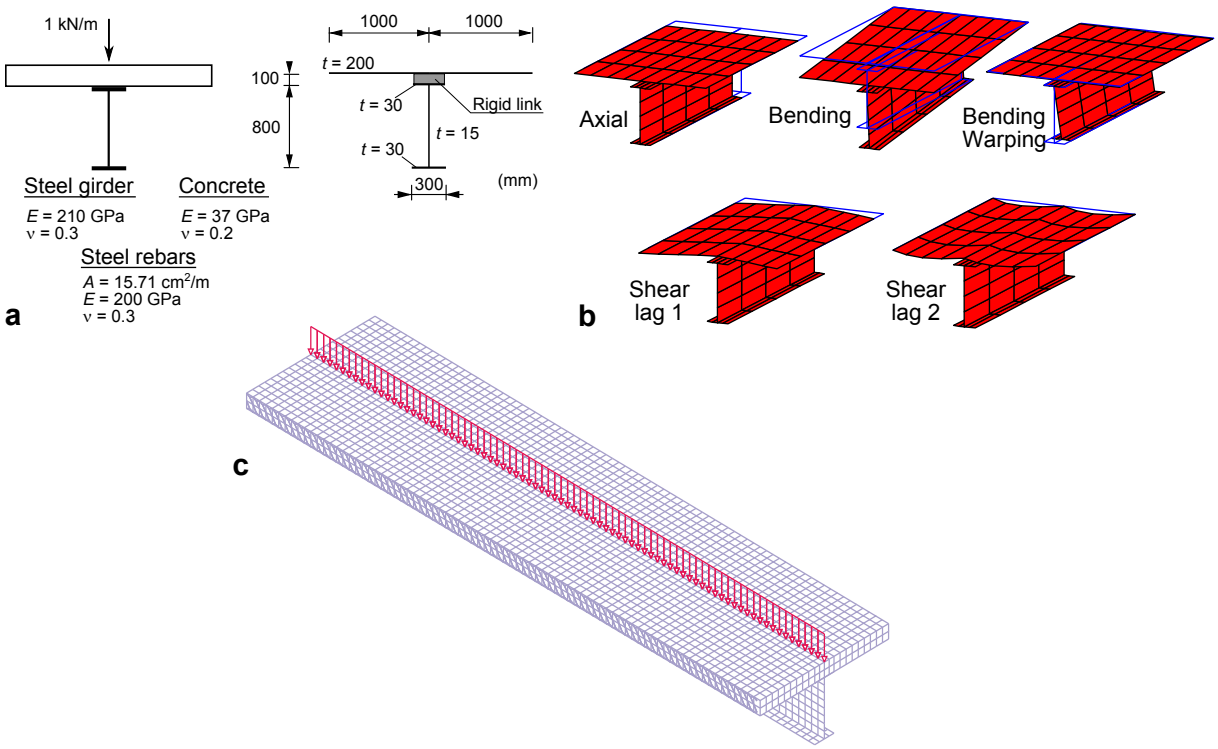

Figure 4: Example 2: (a) cross-section geometry, loading, material parameters and equivalent "frame" for the GBT cross-section analysis, (b) deformation modes and (c) shell/truss/solid finite element model.

assumed positive)

$$\sigma = \frac{E_c \varepsilon}{1 + \left(E_c/(\sigma_c/\varepsilon_c) - 2\right) \varepsilon/\varepsilon_c + \left(\varepsilon/\varepsilon_c\right)^2}. \tag{8}$$

In this case, numerical integration in the concrete flange is performed with 5 Gauss points along z.

The graph in Fig. 6(c) plots the GBT results (18 equal length elements), as well as those reported in [8, 9], showing a very good match, although the collapse load obtained in the test is underestimated by 2.6%. For illustrative purposes, the deformed configurations of the beam at the maximum load are shown in Fig. 6(b).

3.4 Example 4

The last example combines non-linear material behaviour and shear deformation. The beam previously analysed in example 2 is again analysed, with the non-linear material parameters indicated in Fig. 7(a).

The GBT analyses are carried out with 8 equal length finite elements, $\beta = 1$ and considering either (i) only the axial extension and bending modes (no shear deformation, 31 d.o.f.) or (ii) all modes shown in Fig. 4(b) (with shear deformation in the concrete

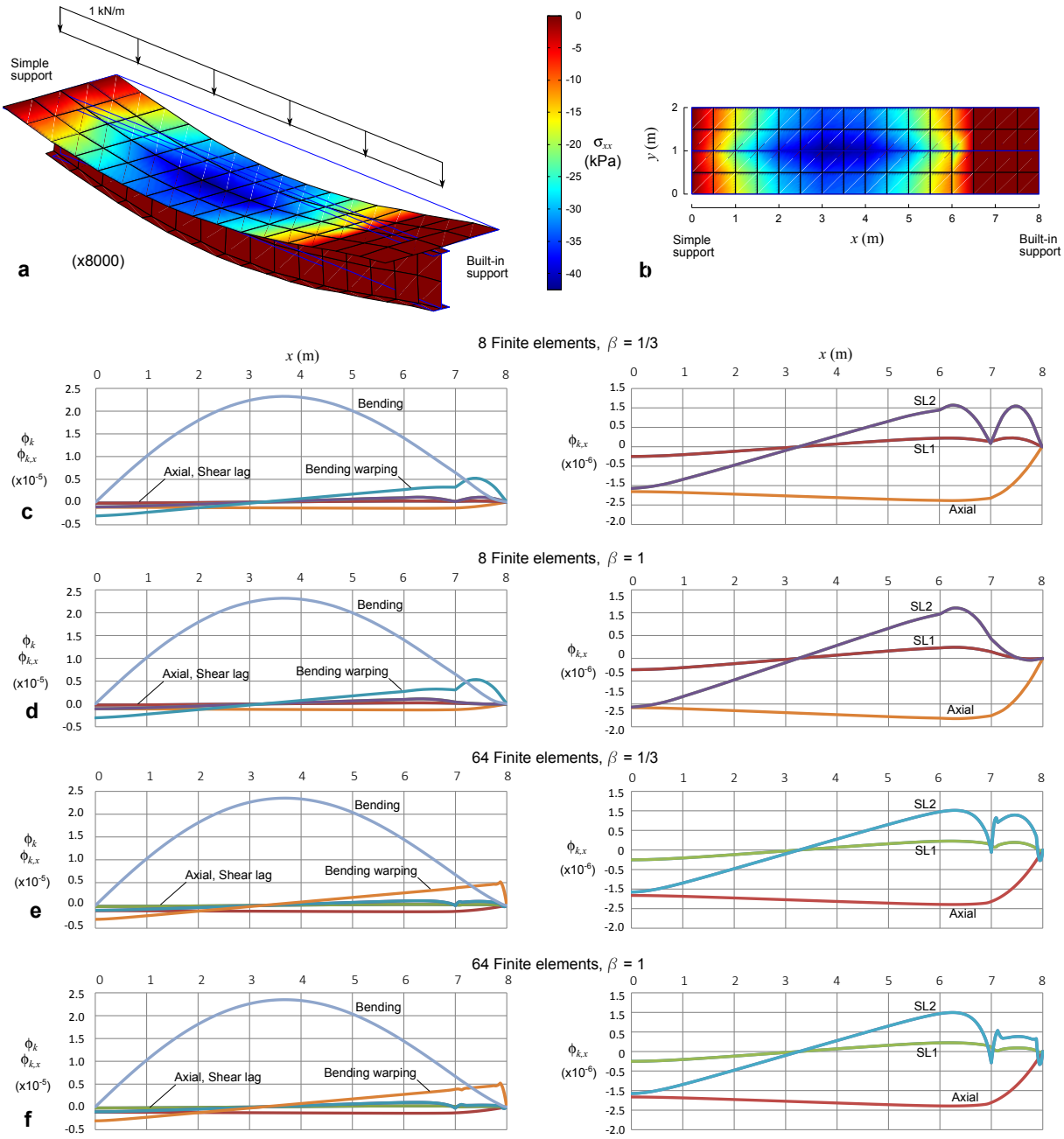

Figure 5: Example 2: (a-b) deformed configuration and stresses in the concrete slab, (c-f) mode amplitude functions along x, for 8/64 finite elements and $\beta = 0.333/1.0$.

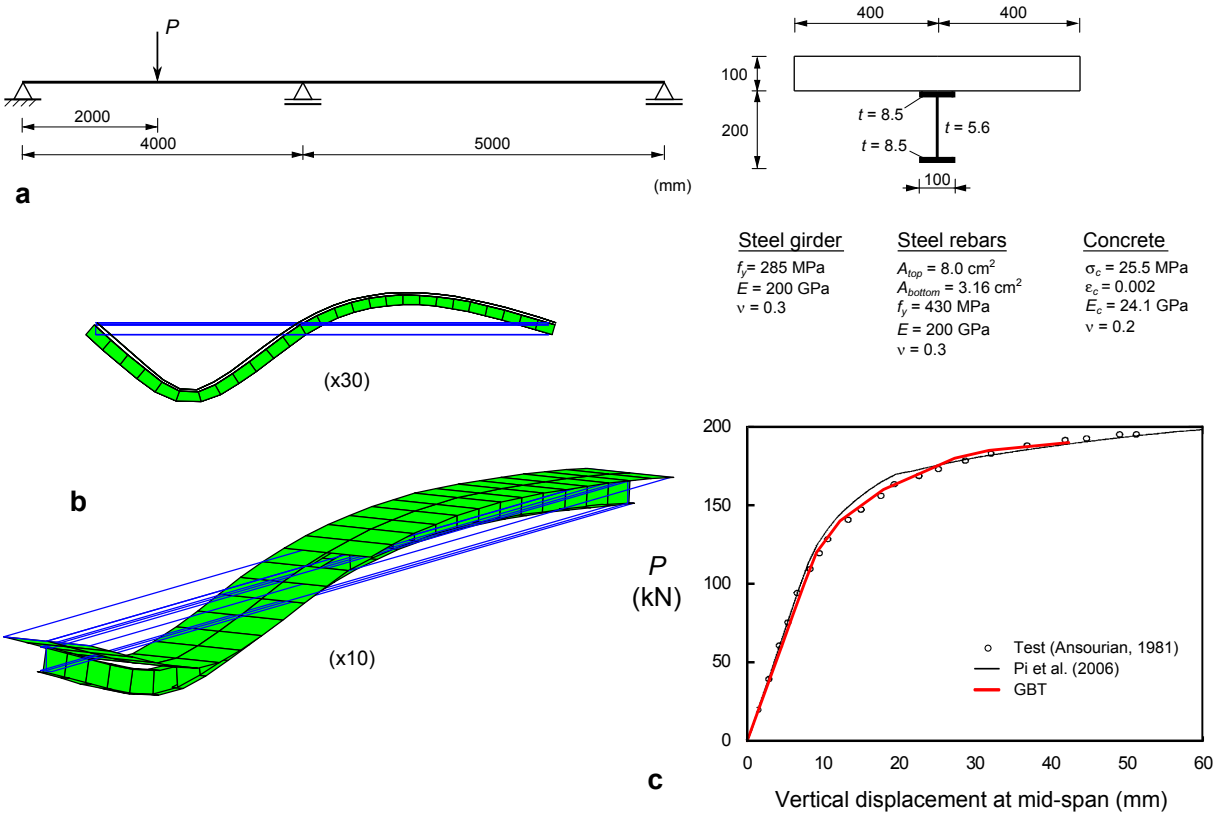

Figure 6: Example 3: (a) loading and geometric/material parameters; (b) deformed configurations at collapse; (c) load-displacement graph.

and steel web, 111 d.o.f.). The concrete material law is given by Eq. (8). Again, 5 Gauss points along z were considered in the concrete flange.

The ADINA model with shell/truss/solid elements did not provide an adequate load-displacement path, due to convergence problems at very early stages of the loading. This motivated the use of ATENA [10], which is specifically towards reinforced concrete structures and contains shell elements capable of incorporating concrete material behaviour and smeared reinforcement. The finite element model adopted is shown in Fig. 7(c) and involves over 8000 d.o.f., even though advantage was taken of the cross-section symmetry.

The deformed configurations at collapse, obtained with GBT and ATENA, are shown in Fig. 7(b) and (d), respectively, and a reasonable good agreement between them is observed. Note that significant shear deformation in the steel web occurs near the built-in end (see also the mode amplitude graph), illustrating the usual bending/shear plastic interaction in built-in supports.

The load-displacement curves obtained with ATENA and GBT (with all modes) show an excellent agreement, although the latter extends further, thus predicting a higher load-carrying capacity. The GBT analysis without shear modes lead to completely wrong

results.

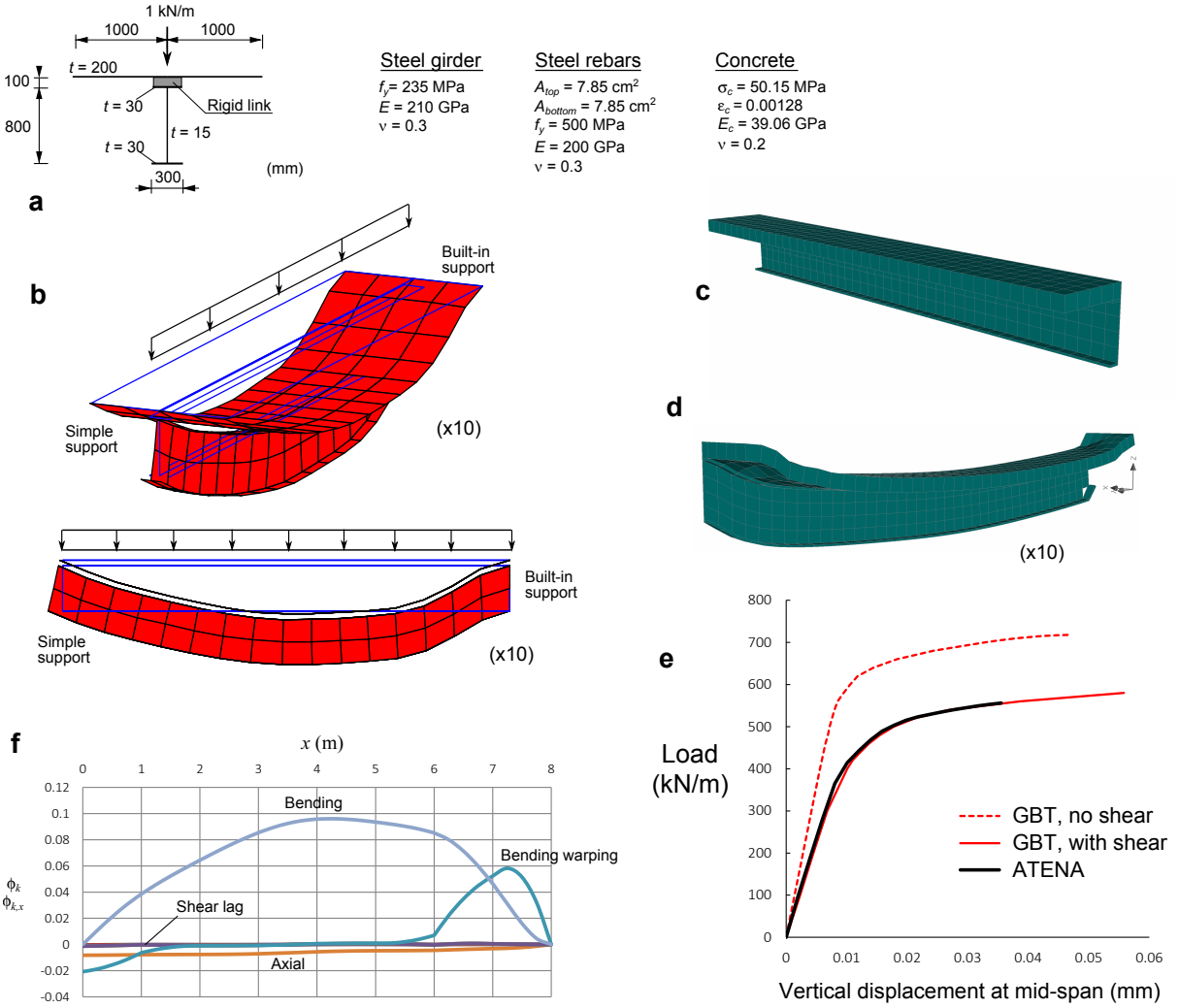

Figure 7: Example 4: (a) loading and geometric/material parameters, (b) GBT deformed configurations at collapse, (c) ATENA shell model, (d) ATENA deformed configuration at collapse, (e) load-displacement graph and (f) mode amplitude functions along x.

4 Concluding remarks

This paper presented a GBT-based finite element which is capable capturing the materially non-linear behaviour of steel-concrete composite beams, namely concrete non-linear behaviour under compression and cracking, shear deformation effects in the concrete flange (shear-lag) and in the steel beam, as well as plasticity in the steel beam. Several illustrative examples were presented, where the GBT-based results were compared with those

obtained using shell/solid finite element models and also with available experimental results. In all cases, a very good agreement was found, even though only a relatively small number of deformation modes were included in the GBT analyses.

REFERENCES

[1] R. Gonçalves and D. Camotim. Steel-concrete composite bridge analysis using Generalised Beam Theory. *Steel and Composite Structures*, Vol. **10**(3), 223–243, 2010.

[2] R. Gonçalves and D. Camotim. GBT-based Finite Elements for Elastoplastic Thin-Walled Metal Members. *Thin-Walled Structures*, Vol. **49**(10), 1237–1245, 2011.

[3] R. Gonçalves and D. Camotim. Geometrically Non-Linear Generalised Beam Theory for Elastoplastic Thin-Walled Metal Members. *Thin-Walled Structures*, Vol. **51**, 121–129, 2012.

[4] R. Schardt. *Verallgemeinerte Technische Biegetheorie*, Springer-Verlag, 1989.

[5] D. Camotim, C. Basaglia, R. Bebiano, R. Gonçalves and N. Silvestre. Latest developments in the GBT analysis of thin-walled steel structures. *Proc. Int. Coll. Stability and Ductility of Steel Struct.*, Rio de Janeiro, Brazil, E. Batista, P. Vellasco and L. Lima (eds.), 33–58, 2010.

[6] F. Gruttmann, R. Sauer, W. Wagner. Theory and numerics of three-dimensional beams with elastoplastic material behaviour. *Int. J. Numer. Meth. Engng.*, Vol. **48**, 1675–1702, 2000.

[7] K. J. Bathe, ADINA System, ADINA R&D Inc., 2010.

[8] P. Ansourian. Experiments on continuous composite beams. *Proc. Inst. Civ. Eng.*, Vol. **71**(2), 25–71, 1981.

[9] Y. Pi, M. Bradford, B. Uy. Second order nonlinear inelastic analysis of composite steel-concrete members. II: Applications. *Journal of Structural Engineering*, Vol. **132**(5), 762–771, 2006.

[10] ATENA version 5, Cervenka Consulting, 2013.